Rheol Acta (2017) 56:635–648
DOI 10.1007/s00397-017-1025-0

ORIGINAL CONTRIBUTION

Linear and non-linear nature of the flow of polypropylene filled with ferrite particles: from low to concentrated composites

Martha Margarita Rueda [1,2] · René Fulchiron [1] · Grégory Martin [2] · Philippe Cassagnau [1]

Received: 15 January 2017 / Revised: 31 May 2017 / Accepted: 15 June 2017 / Published online: 29 June 2017

Abstract The flow behavior of a filled suspension consisting of ferrite particles suspended in a polypropylene matrix with and without the addition of a commercial dispersant (Solplus DP310) was studied. The composites were filled with 10, 20, 30, and 40 vol.%. Both capillary and parallel disk rotational flows were employed. On the one hand, dynamic results confirm general trends found for highly concentrated systems. The higher is the filler level, the lower is the linear viscoelastic domain. When adding the dispersant agent, it was shown a larger linear viscoelastic domain, lower moduli values and thus, lower viscosity. Also, the critical strain, G' and G'' showed a power law dependency on the volume fraction. On the other hand, the capillary results showed no dependency of the flow properties on the die. Thus, no slip of the suspension at the wall was observed. Actually, this experimental finding elucidated that the significant decrease on viscosity produced by the addition of the dispersant agent at 40 vol.% is principally due to lubricant effects and not at all to slip contributions. The results also reveal three distinct flow regimes. Low, moderate, and high shear rates lead to different microstructure under flow.

Keywords Concentrated composites · Thermoplastic matrix · Rheology · Dispersant · Viscosity · Ferrite particles

✉ Philippe Cassagnau
philippe.cassagnau@univ-lyon1.fr

[1] Univ-Lyon, Université Lyon 1, Ingénierie des Matériaux Polymères, CNRS, UMR 5223, 15 Bd Latarjet, 69622 Villeurbanne Cedex, France

[2] HUTCHINSON Research Center, Rue Gustave Nourry–B.P. 31, 45120 Chalette-sur-Loing, France

Introduction

Understanding the rheological behavior of highly filled (HF) materials gain a lot of interest in many industrial applications such as magnetic materials (Saini et al. 1986; Fiske et al. 1997), thermal pastes (Feger et al. 2005), batteries (Voillequin et al. 2013), solid propellants (Azoug et al. 2014), electrically conductive compounds (Boudenne et al. 2005), and the elaboration of ceramic materials (Lusiola et al. 2014), among other applications (Rueda et al. 2017). The concentration of solids in such applications need to be maximized to be as close as possible to the maximum packing fraction of solids (ϕ_m), generally exceeding 60 vol.% of the particulate phase (Kalyon and Aktaş 2014; Rueda et al. 2017). Such high quantity of fillers strongly increases the mixture viscosity and thus the elaboration process becomes extremely difficult to control (Rueda et al. 2017). In addition, polymer-filler and filler-filler interactions may lead to agglomeration in the suspensions, defining the resultant morphology and thus the rheology of the materials (Rueda et al. 2016). For these reasons, most of these materials present dispersants (amphiphilic additives) in their formulations. They are claimed to avoid sedimentation of particles, to prevent agglomeration process and to produce low viscosity suspensions (Osman et al. 2004; Zürcher and Graule 2005; Ried et al. 2008; Fall et al. 2013; Rueda et al. 2016).

It is generally known that all metal and metalloids oxides particles are covered by hydroxyls (−OH) or ions groups which will determine the adsorption processes that take place onto the surface of particles (Armistead et al. 1969; Potanin and Nelson 2003). The most common used dispersants in molten polymers are fatty acids, amine, and amide acids. Fatty acids, in particular, present a carboxyl functional group (COOH), which is able to being adsorbed onto the particle surface either by creating chelate complexes or hydrogen bonds (Hidber et al. 1997; Potanin and Jr 2003; Zürcher and Graule 2005). Thus, dispersants coat and

modify the interparticle potential by increasing the particle charge or by building up a steric barrier between particles (Moloney et al. 1995). In particular, a commercial dispersant, Solsperse 3000 (S3000) which principally consists in a penta-(12-hydroxystearic acid) oligomer, has been successfully used to disperse zirconia (YZS) (Moloney et al. 1995; Zürcher and Graule 2005), hydroxyapatite powder (Gao et al. 2011), and ferrite particles (Burnat et al. 2010) in organic and semi-organic media (low molar mass liquids). Its efficiency has been demonstrated over a wide number of dispersants, including fatty acids, e.g., palmitic, stearic, and oleic acid; fatty amines and molecules with hydroxyl groups (Moloney et al. 1995; Zürcher and Graule 2005; Gao et al. 2011). This has been attributed to its effectiveness of the chelating anchoring group to bind on metal and oxide surfaces, in addition to the higher steric effect produced by its long carbon chain (66 carbon chain which is at least 10 nm long) (Moloney et al. 1995; Zürcher and Graule 2005). Despite the efforts, the influence of these additives on the melt flow behavior is less well-known and has been less studied. Molten polymers are highly entangled in the melt which results in a quite different behavior (Denn 2001), as well as, different diffusion and mechanism of adsorption compared to what happen in a low molar mass medium.

In our recent work (Rueda et al. 2016), we demonstrated that a similar dispersant, Solplus DP310 (SDP310), was able to stabilize the rheological properties of ferrite particles suspended in polypropylene. First, we have shown that the structure of such composites were not stable over time. Micro-structural changes were manifested by a sharp increase on the storage modulus (G'), resulting in a solid-like behavior at the end of the experiment. This manifestation was particularly important under very low shear deformations in the linear viscoelastic domain (LVD). When adding the dispersant, SDP310, it was shown that this drastically hinders the agglomeration process, impeding the creation of the particle network.

From a process point of view, HF polymers definitely need the addition of a dispersant agent to broaden the process window and to facilitate the elaboration process, as long as it does not modify the final properties of the composite. The addition of particles dramatically changes the viscoelasticity of polymer melts (Ariffin et al. 2006; Cassagnau 2013) and strongly increases the viscosity of the mixture (Kaully et al. 2007). All this recreates the perfect conditions for processing difficulties, resulting in flow instabilities. When considering quantitative analysis of polymer processing, the flow-boundary condition is a fundamental assumption to describe laminar flow (either no slip at the wall or slip condition) (Bravo et al. 2004; Kalyon and Aktaş 2014). Wall slip phenomenon has been claimed to be ubiquitous and the controlling phenomenon of the flow behavior of highly concentrated suspensions (Yilmazer and Kalyon 1989; Kalyon 2005; Gulmus and Yilmazer 2005). In HF polymers field, the wall slip velocity has been found either to increase (Gulmus and Yilmazer 2005) or decrease (Li and Wolcott 2005; Hristov et al. 2006; Haworth and Khan 2005), when adding particles. The slip at the wall has also been shown to appear at a certain value of ϕ/ϕ_m and then to remain relatively independent of such value (Soltani and Yilmazer 1998). There is also evidence of no correlation between flow properties and wall slip. Hence, the slip velocity was found in some studies negligible even at high shear rates in capillary tests (10^3, 10^4 s^{-1}) (Poslinski et al. 1988a; Kaully et al. 2007). In addition, when adding a dispersant or a coupling agent, it is generally believe that unreacted dispersant is likely to migrate to the die wall. Hence, an accumulation of the dispersant agent may occur at the wall, resulting in slip effects, plug flow and, in some cases, the suppression of flow instabilities have been observed (Suwardie et al. 1998; Ahn and White 2004; Haworth and Khan 2005).

This paper presents experimental results of the rheological behavior of a filled polymer up to concentrated regimes. Generally, ferrite suspensions studies use dispersants to stabilize the flow properties (Yang et al. 1986; Dasgupta 1988a, b; Navarrete et al. 1996; Rueda et al. 2016). Therefore, this work revisits important concepts of concentrated suspensions with and without the addition of a dispersant agent; by highlighting the important relationship between the microstructure and the flow.

Materials and methods

Materials

Polymer

The matrix used in this study is a commercial homopolymer polypropylene PPH7060 (PP), provided by Total refining and chemicals. Table 1 summarizes some of its characteristics. A sterically hindered phenolic antioxidant, Irganox 1010 (I) was used as a thermal stabilizer at 1 wt.% based on the weight of the polymer (it protects PP matrix against thermo-oxidative degradation).

Particles

The ferrite powder NK132 (F) was supplied by Toda Kogyo Corp., Japan. These particles are a solid solution of Strontium with a low quantity of Barium Ferrite. The characterization of the particles has been discussed in detail in our recent work (Rueda et al. 2016). Ferrite particles have hexagonal plate shape with an average diameter (d) of 2 μm and 0.5 μm in thickness (l). The aspect ratio is around $p = d/l = 4$.

Dispersant

Different works showed that the commercial dispersant, S3000, has a high potential to reduce the mixture viscosity

Table 1 Characteristics of polypropylene matrix (PPH 7060)

Properties	Method	Value	Unit
Density	ISO 1183	0.905	g/cm^3
$\overline{M}_n - \overline{M}_w$	Size exclusion chromatography	67,300–273,000	g/mol
Melting point (T_f)	ISO 3146	165	°C
Melt flow index	230 °C/2.16 kg	12	g/10 min
η_0 (at 190 °C)	Viscosity at the plateau*	3800	Pa s

* Carreau-Yasuda parameters: rate index (n) = 0.22, characteristic time (λ) = 0.092 s, transition index (a) = 0.47, η_∞ =0 Pa s

in organic liquid media (Zürcher and Graule 2005; Gao et al. 2011; Moloney et al. 1995). Based on these analyses, we compared and chose a new dispersant from its same family. In this work, SDP310 was used as an alternative to S3000. Both dispersants were kindly supplied by Lubrizol, Advanced Materials. SDP310 is a white powder (spheres of $\overline{d}$ = 150 μm) with T_f = 105.5 °C, while S3000 is a waxy paste at room temperature.

SDP310 characterization has been facilitated thanks to Moloney and coworkers (Moloney et al. 1995). They reported S3000 as a pentamer made up of one steric acid unit and four units of poly (12-hydroxy-stearic acid). This oligomer was compared to SDP310 by using thermogravimetric analysis (TGA), attenuated total reflection (ATR) spectroscopy, nuclear magnetic resonance (NMR) spectroscopy, and matrix-assisted laser desorption/ionization time-of-flight (MALDI-TOF) mass spectrometry. Some of these results are shown in Fig. 1a, b shows the TGA measurement performed for both dispersants. As it can be noticed, S3000 presents a monomodal distribution of population of oligomer chains, the population that is present in the largest amount is a penta (12-hydroxy-stearic acid) (Moloney et al. 1995). SDP310 presents three principal populations, one being a penta (12-hydroxy-stearic acid). Figure 1c presents the transmission spectrum for both dispersants in which only SDP310 peaks are identified and attributed to the corresponding functional group. It can be clearly observed that S3000 and SDP310 present very similar chemical structures, despite the huge difference in their physical appearance. Infrared spectra reveal typical features from carboxylic acid with long carbonaceous chain described by the CH_2 stretching and rocking bands. Finally, the chemical composition has been studied by Maldi-tof mass spectroscopy. The waxy S3000 dispersant was easily dissolved in most common solvent compounds; whereas, SDP310 powder was not. A mixture $CHCL_3$/EtOH/H_2O (70/20/10 v/v/v) partially dissolves SDP310; a white color solution was obtained. THF and $CHCL_3$/EtOH/H_2O were chosen as solvents for S3000 and SDP310, respectively. Figure 1d shows the molecule found by Maldi-tof based on (Moloney et al. 1995). The results demonstrated that both dispersants has exactly the same repeating unit ($C_{18}H_{34}O_2$). This technique also confirmed very exactly both extreme units: ($C_{18}H_{35}O_1$) and (OH). The degree of polydispersity (DP) goes from 1 to 10 for SDP310 and 1 to 12 for S3000. Nonetheless, results are not quantitative for samples with very large distribution, as in our case. NMR corroborated the latter results, without giving additional quantitative information again due to the high polydispersity of population.

On the basis of these results, it can be stated that SDP310 is a poly (12-hydroxy-stearic acid) with a high dispersity index (DP = 1 to10). SDP310 powder was chosen for this study due to its high thermal stability and ease of use in extrusion process. The powder state facilitates the handle of the product unlike waxy physical state.

Mixing and sample preparation

The mixing of the components was performed by extrusion process by means of a Leistritz ZSE-18, fully intermeshing co-rotating twin-screw extruder. The barrel length over barrel diameter, L_b/D_b, was 60 and the barrel diameter was 18 mm. The operating conditions were fixed at 190 °C, a speed of 800 rpm, and throughput of 3 kg/h.

A pre-mixing of the powders (ferrite +2 wt.% SDP310) and the matrix (PP granulates +1 wt.% Irganox 1010) was manually performed. Then, composites with filler levels from 10 to 40 vol.% were performed, granulated and then shaped into rheometer disks by injection molding by means of a Babyplast 610P, Alecop at 190 C. Collected disks and pellets were characterized by rotational and capillary rheometry, respectively. Samples with and without the dispersant agent were prepared. The dispersant concentration was fixed at 2 wt.% based on the weight of fillers. The screw profile used in this study is illustrated in Fig. 2. This may be considered as a soft screw profile, principally because it does not present any reverse element and its kneading blocks are positioned with favorable feed angles.

Rheological characterization

Dynamic rheological test

Linear viscoelasticity characterization was performed by employing a stress-controlled Discovery Hybrid Rheometer (DHR), TA instruments. All measurements were performed

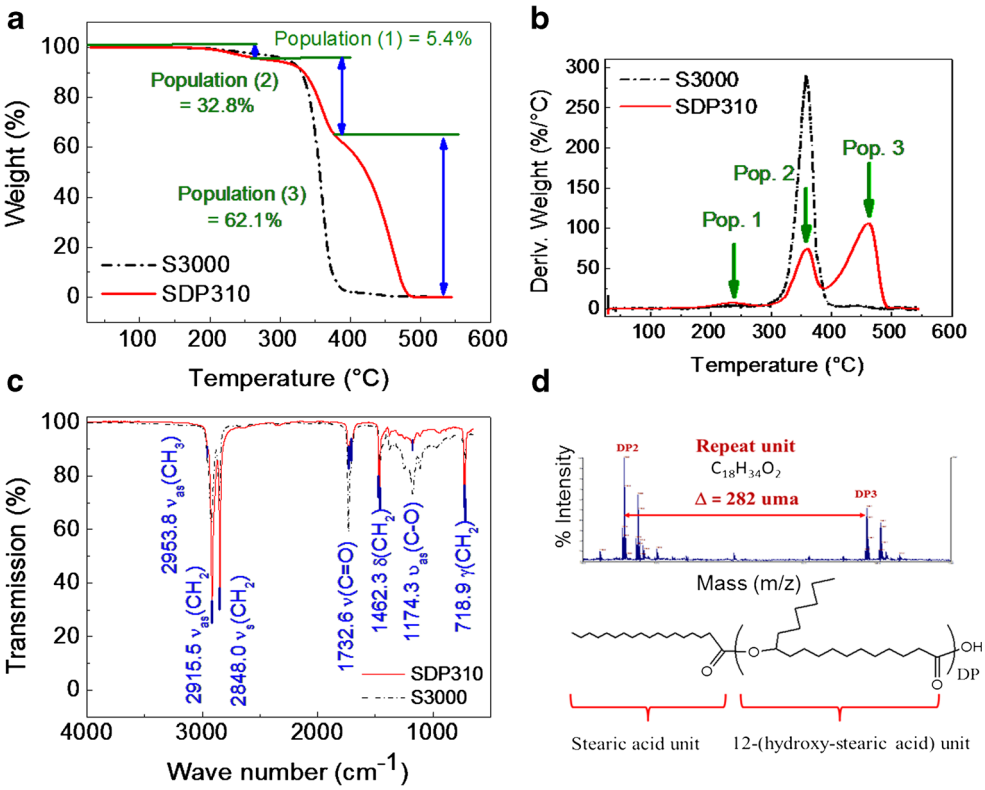

Fig. 1 Solplus DP310 (SDP310) dispersant characterization, considering as reference S3000 reported by (Moloney et al. 1995). (**a**) Normalized weight loss curves and (**b**) derivative weight loss curves of S3000 and SDP310. From 25 °C to 550 °C at 10 °C/min under Helium. (**c**) Infrared transmission spectra for both dispersants. Denoted peaks are shown only for SDP310 with their respective assignment, where: *as* asymmetric, *s* symmetric, υ stretching, δ bending, and γ rocking. (**d**) Repeat pattern ($C_{18}H_{34}O_2$), as well as the oligomer molecule found by Maldi-tof technique for both dispersants

at 190 °C under nitrogen atmosphere, using a plate-plate geometry (diameter = 25 mm). The gap was fixed at 1800 μm. A sample conditioning was performed before all the tests to erase and impart an initial state of dispersion to the sample. The global protocol consisted in five steps: (1) soak time of 300 *s* in order to enable the sample to relax stresses due to the loading, (2) pre-shearing of 0.5 s^{-1} for 160 s and (3) annealing step in which the sample was maintained under quiescent conditions for 1 h. (4) A frequency sweep was performed, followed by (5) a strain sweep. The annealing step was performed to enable the structuring of the material to attain a certain equilibrium. Frequency sweeps were performed in the linear viscoelastic domain under the strain amplitude range between 10^{-3}–10^{-4} according to the filler level. Oscillatory strain sweeps were performed at fixed frequency of 1 rad/s, from 6×10^{-6} to 2 of deformation (γ).

Capillary rheometry

A twin-bore capillary rheometer (RH7, Rosand, Malvern) was used to study the shear flow behavior of such composite melts. The diameter of the bore was 15 mm. Steady shear flow properties were collected from 1 s^{-1} to 4×10^4 s^{-1} at 190 °C. To maintain consistency between the tests, a pre-conditioning was applied before running the experiments. Such pre-conditioning principally enables a good contact between the piston and the melt composite, lets the whole sample reach the thermal equilibrium, and

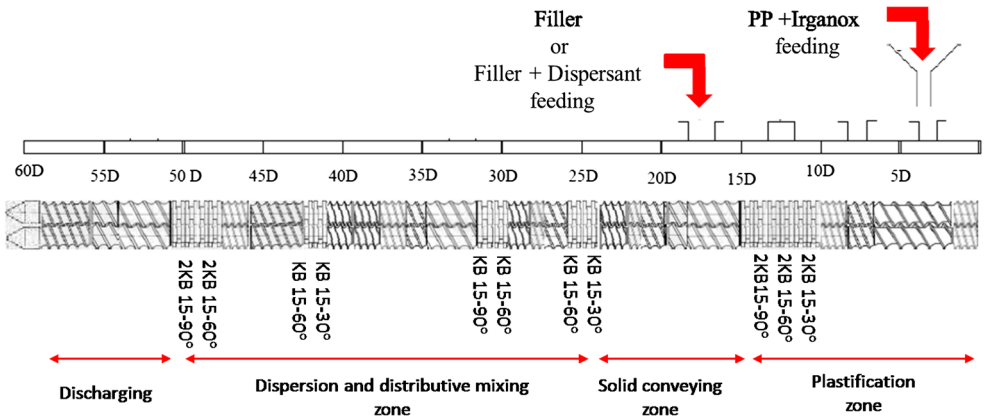

Fig. 2 Schematic representation of the soft screw profile used in this study. Leistritz ZSE18, $L_b/D_b = 60$. Kneading blocks (*KB*) are characterized by 15 mm axial length and 30° stagger angle

removes trapped air bubbles. It consisted in 2 cycles of compression (according to the transducer) and soak time (5 and 4 min).

First, wall slip was analyzed by using three different dies with capillary length over diameter, L/D = 10 and entry angle of 180° (L/D = 10/1, 15/1.5, and 20/2 mm/mm). The obtained data were further processed according to Bagley correction. The orifice die was used to perform this correction (L = 0.25, D = 1, 1.5, 2). The pressure drops through this orifice was subtracted from the measured values of pressure. This is simultaneously performed during the measurement by using the double capillary system with orifice die. Second, the shear viscosity the composite was analyzed by using a die with L/D = 20/1 and entry angle 180°. The Bagley correction was again applied. The Rabinowitsch correction did not change in any aspect of the behavior of the filled composites but rather slightly enhance the differences. We thus decided to show the apparent shear rate to be consistent to the wall slip analysis.

Morphological characterization

The state of dispersion has been observed by scanning electron microscopy (SEM) and tomography. SEM observations have been performed by means of a Quanta 250 SEM under high vacuum; an acceleration voltage of 10 kV with an electron backscatter diffraction (EBSD) detector. Prior to observations, the samples were cryo-cut and metallized by using a Bal-Tec MED 020 Coating System. Sputter coating was applied under 35 mA, and a 10 nm layer copper was deposited. A quartz layer device was used for measuring the layer thickness.

Tomography (Nanotomography I-580) observations were also conducted to examine the state of dispersion. We were able to quantify the presence of agglomerates with a diameter >10 μm for 2 samples. Composites filled with 20 vol.% without and with the addition of the fatty acid were analyzed. The measurements were performed under 70 kV voltage, 90 μA intensity, and 1250 ms of exposition time. The disk samples (diameter = 25 mm, thickness = 2 mm) obtained by injection molding process were cut into rectangular sample. The dispersion analysis has been performed over an identical volume of 45.5 mm^3 for the 2 samples. The obtained 3D tomograms were threshold, binarized, and the voxels which constitutes the agglomerates were quantified, giving as a result the agglomerate volume. Assuming spherical agglomerate shape, the equivalent diameter (D_{eq}) is calculated as $D_{eq}=(6V//\pi)^{1/3}$. According to this method, we are able to calculate the median diameter by number (D_n).

Results and discussion

In our recent work (Rueda et al. 2016), we have covered the structuring over time of these materials at very low deformations, essentially in the LVD for samples filled with 15 and 20 vol.%. Here, we will discuss different aspects on the linear and non-linear nature of the flow of more concentrated ferrite composites. Data were collected after 1 h structuring in dynamic rheology and in the steady state in capillary rheology. No sign of structuring has been noticed in capillary rheometry.

Some abbreviations will be used in the following. Samples will be denoted by their process, their filler level and their formulation. For instance: EF20 and EFD20, whose letters mean E extrusion, F ferrite, D dispersant and the number corresponds to the filler level in volume percentage.

Morphology observation

Agglomerates whose size ranges between 10 and ~100 μm were quantified for a sample filled with 20 vol.% with and without dispersant. Figure 3a–d shows some 2D images obtained by 3D tomographs. As a general observation, these images showed a homogenous gray zone with some dispersed white zones. The homogenous zones are represented by the Fig. 3e–f, in which particles are well dispersed through the matrix, while, white zones are displayed in Fig. 3g. Such white zones correspond to very dense zones of particles, thus to one agglomerate. Agglomerates seem to be uniformly distributed through the observed sample.

Table 2 sums up some important information obtained by image analysis provided by tomography method. First, for an identical volume, the average diameter of the agglomerates (D_{eq}) is about 26–27 μm for each one of the formulations (EF20, EFD20). Second, very few but huge agglomerates over 100 μm were found for both samples. Finally, there is not enough evidence to draw a significant conclusion to differentiate the state of dispersion between both formulations.

Moreover, it is also important to remark that extrusion-injection molding samples do not present entrapped air bubbles, unlike samples produced on a Haake melt blender and then shaped by hot-press (Rueda et al. 2016). This is extremely important because it has been shown that entrapped air may induce slip at the wall (Aral and Kalyon 1995; Kalyon and Aktaş 2014) and may affect the stability of HF suspensions (Feger et al. 2005). In tomography, entrapped air would be indicated by a very low dense zone in black, according to the grayscale density.

Dynamic rheology

Figure 4 displays frequency sweeps performed for the neat matrix (EPPI) and samples filled from 10 to 40 vol.% with and without the addition of the dispersant agent. It is important to remember that these tests were obtained after a pre-shearing and 1 h of annealing time, in which the microstructure evolves (Rueda et al. 2016). The tests were

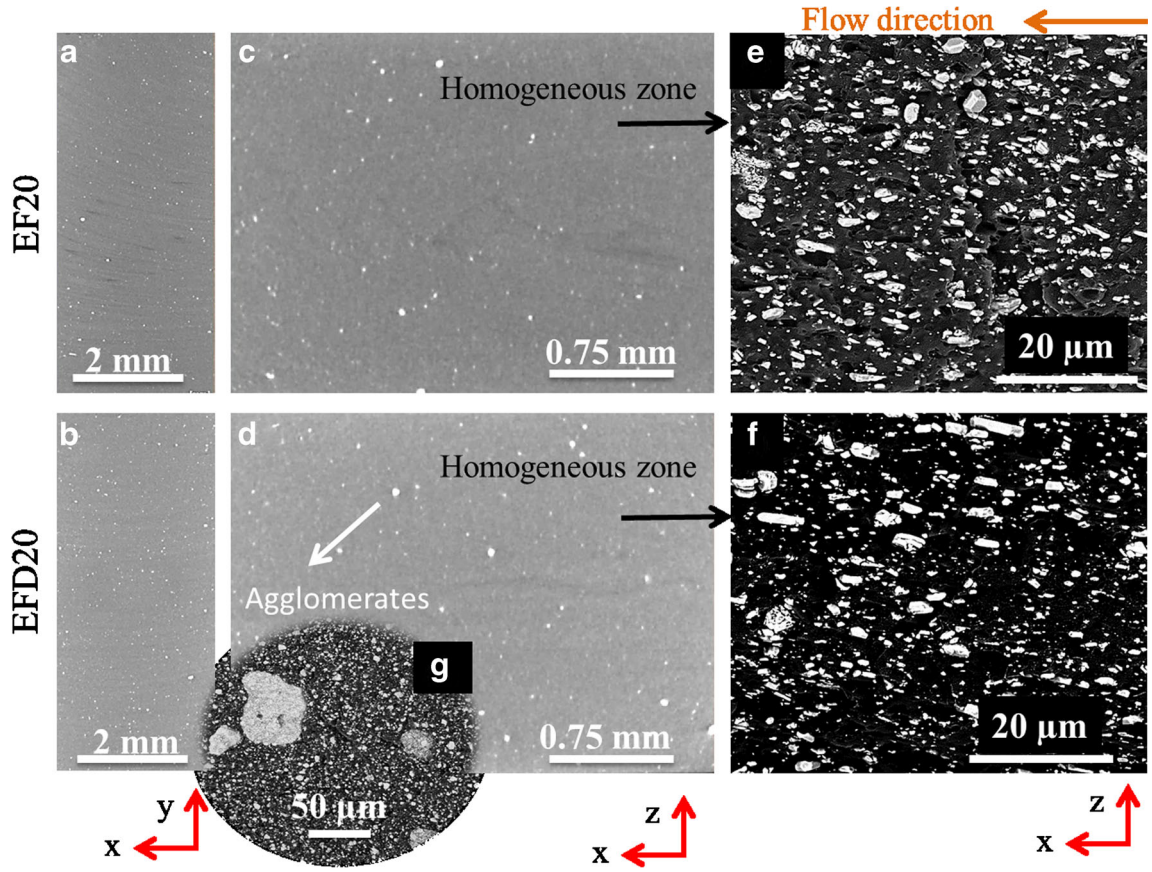

Fig. 3 State of dispersion observed by tomography and SEM microscopy for samples EF20 (a, c, e) and EFD20 (b, d, f, g). Tomography (a, c, b, d) was performed over rectangular pieces of 3 mm width, 2 mm height, and 7.7 mm length under 55 kV and 150 µA. SEM microscopy (e, f, g) was performed under 10 kV, high vacuum (10^{-6}), and BSED detector. x, y, and z axis represent width, length, and height of the rectangular piece where z corresponds to the thickness and x the flow direction during the injection molding process

performed in the LVD and further verified with a consecutive strain sweep.

From Fig. 4a, the percolation threshold (ϕ_c) can be evidenced between $0.1<\phi_c<0.2$, due to the change in the flow

Table 2 Agglomerate size characterization by tomography method. Studied system = EF20 and EFD20, 45.5 mm^3 under 55 kV and intensity of 150 µA. D_n = median diameter by number

Sample	EF20	EFD20
n	2821	2946
Maximum D_{eq} (µm)	132	102
Mean D_{eq} (µm)	27	26
$D_n(0.2)$ (µm)	<20	<20
$D_n(0.8)$ (µm)	<35	<35

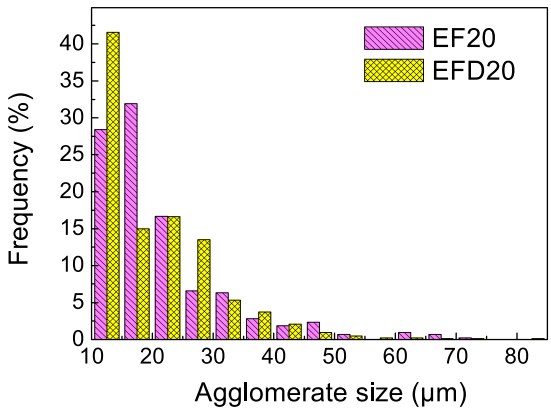

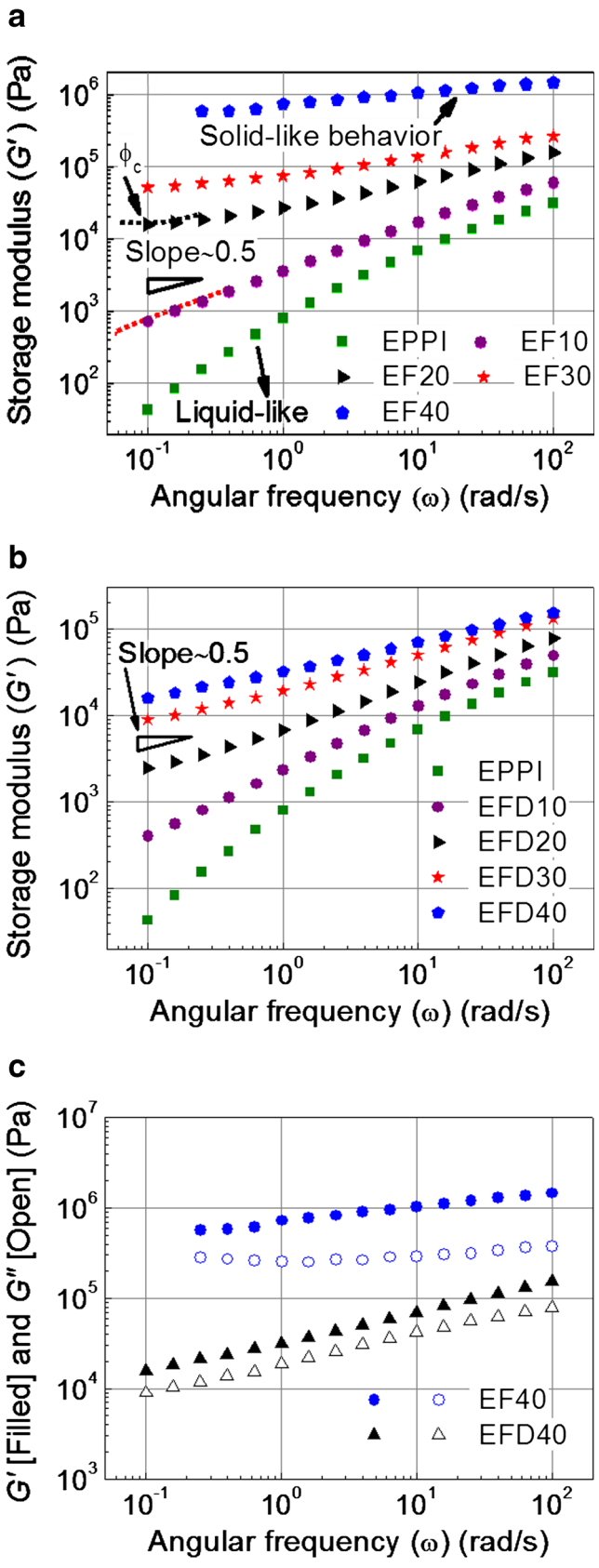

◀ **Fig. 4** Frequency sweep for samples filled with 0, 10, 20, 30, 40 vol.% (**a**) without and (**b**) with the addition of 2 wt.% of SDP310. Such tests were performed by using parallel plate geometry after 1 h annealing time, under nitrogen, 190 °C and (10^{-4}–10^{-3}) of strain. *Dashed lines* were put to guide the reader. (**c**) Comparison between EF40 and EFD40

regime. This means that a change in the plot curvature occurs, necessary passing by the moment which describes the material percolation ($G'(\omega)\alpha\ G''(\omega)\alpha\ \omega^{0.5}$) (Rueda et al. 2016). The percolation indicates the existence of strong links among particles, forming microscopic structures. For disk-like particles, ϕ_c has been shown as being inversely proportional to the aspect ratio, $\phi_c = l/d \approx 0.25$ (Kim et al. 2010; Franceschini et al. 2014). Besides this, a geometric percolation obtained by two-dimension analysis is given by $\phi_c = \phi_m/p$ (Gassiot-Talabot 2015), where p is the aspect ratio and ϕ_m the maximum packing fraction defined as ϕ_m=bulk density/true density (Poslinski et al. 1988b). In our case, $\phi_m = 0.72$, and thus $\phi_c = 0.18$. We can indeed state that the physical percolation lies between $0.18 < \phi_c < 0.25$, which in fact supports our observation in Fig. 4a. Saini et al. also reported similar percolation threshold ($0.25 < \phi_c < 0.30$) for ferrite particles with comparable average particle size (Saini et al. 1986).

When the dispersant agent is added, the viscoelastic behavior is changed and the moduli values are highly reduced and thus the viscosity of the mixture (Fig. 4b, c.) shows the comparison between the highest filled materials. EF40 presents a completely solid-like behavior, while EFD40 shows a gel behavior ($G' > G''$ and log G' //log G'') which still has fluidity.

After each frequency sweep, a strain sweep was performed. Figure 5 shows several important trends which are well-known in the HF suspension field. First, the maximum strain to which the LVD extends decreases with increasing the filler level (ϕ) (Barnes 2003) as shown Fig. 5a. Such a decrease of the LVD is interpreted by considering that, when increasing the filler concentration, admittedly inter-aggregate interactions become more abundant, leading to a higher modulus, however, the probability of rupture is also increased so that the network becomes more brittle. This means that, very gentle deformations are transmitted by the connecting paths which in turn produce a particle rearrangement wherever is favorable, breaking the linearity. Thus, the mechanism that governs the onset of non-linearity can be interpreted by considering two regimes: above and below ϕ_c. Above ϕ_c, it can be understood as the rupture of the relatively weak bonds of the particle network (Shih et al. 1990). Below this limit, matrix contribution dominates and so chain disentanglements together with rupture of filler interactions control the phenomenon (Cassagnau 2003). Second, the addition of particles considerably increases both storage (G') and loss modulus (G''), being the effect on G' greater than the effect on G'' (Walberer and McHugh 2001). Finally, strong strain-dependence of the dynamic viscoelastic properties has been also reported in HF

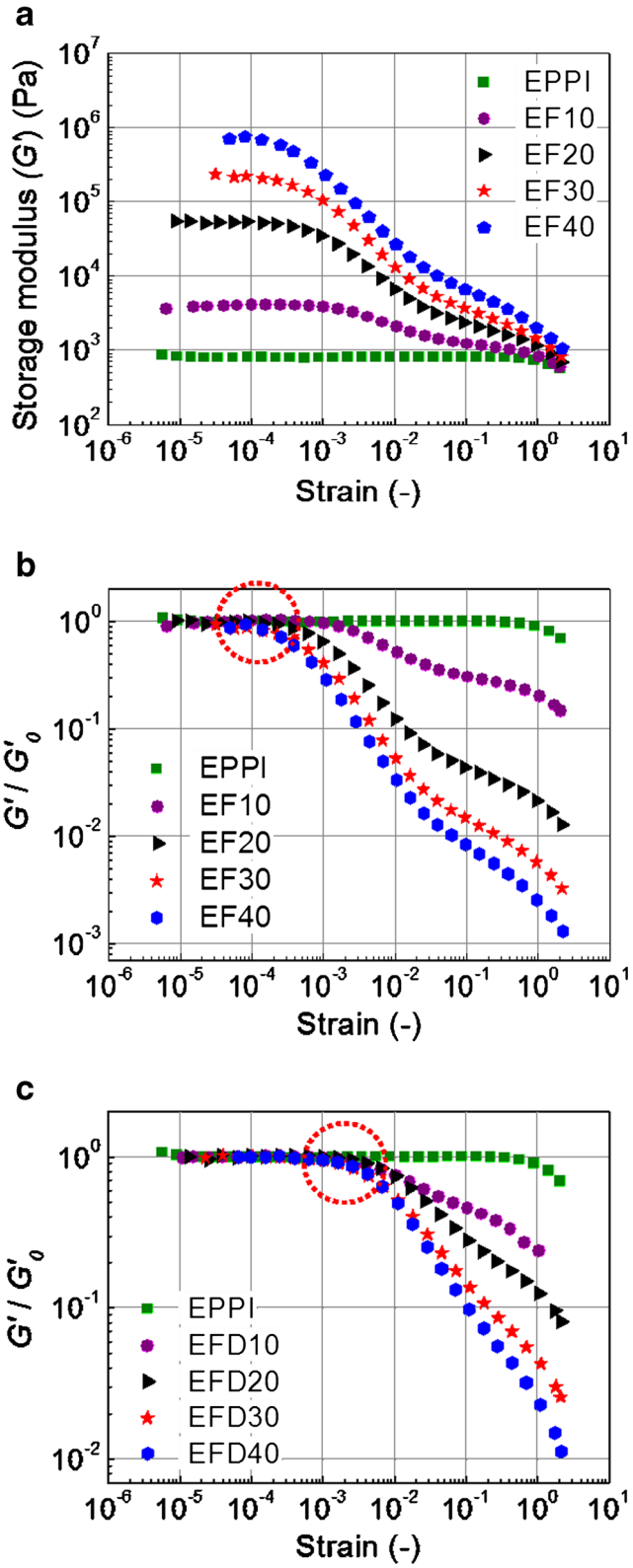

Fig. 5 Strain amplitude sweep from 6×10^{-6} to 2 of deformation (**a**) for composites filled up to 40 vol.%. Normalized values of G'/G'_0 (**b**) without and (**c**) with the addition of the dispersant agent. Tests were performed by using plate/plate geometry after frequency sweeps, under nitrogen, 190 °C and 1 rad/s. *Circles* depict the onset of non-linearity

suspensions (Feger et al. 2005; Merabia et al. 2008). Such dependence is known as the Payne effect, in which the moduli drastically drop when increasing the deformation as it can be clearly evidenced in Fig. 5. The more the filler level is, the larger the amplitude of Payne effect is.

It is important to remember that, at low γ, particles interactions are more visible and at high γ, hydrodynamic interactions predominate over interparticle interactions. For this reason in Fig. 5a, at high γ the behavior converges to the matrix flow behavior (Vermant et al. 2007). So, only very slight differences are visible in such zone ($\gamma > 1$).

Figure 5b, c shows the storage modulus (G') normalized by the storage modulus at the plateau (G'_0) for all the composites. The addition of the dispersant agent drastically changes the viscoelastic behavior of the suspension, extending the limit of linearity for all concentrations as shown by the circle. This is attributed to the fact that lower interparticle interactions result from formulation with fatty acid, conducing to a screen effect between particles.

The critical strain value $\gamma_c = f(\phi)$ is somehow difficult to determine. In order to observe the real decrease in the moduli, it is preferable to plot semi-log graphs of G' and G'' vs $\log(\gamma)$. However, it is even better to establish a limit condition as proposed by (Shih et al. 1990), in which γ_c has been defined as the point beyond which G' deviates more than 5% from its maximum value. This condition has been used in this work for all samples, except for EF30 and EF40. Such composites presented almost no LVD at the lowest strain sensitive of the rheometer. Thus, γ_c and G'_0 were extrapoled from the semi-log plots.

Above the percolation threshold, the critical strain and the storage modulus exhibit a power-law behavior with respect to ϕ, in which $\gamma_c \sim \phi^{-3.4}$, $\gamma_c \sim \phi^{-1.3}$ for formulations EF and EFD, respectively (Fig. 6a). Such dependence is much stronger for samples without the dispersant. The power law exponents for the elastic character of the fractal network were obtained by plotting the modulus at the plateau (G_0) over the matrix plateau modulus ($G_{0,m}$) as a function of ϕ, thus $G'_0/G'_{0,m} \sim \phi^{3.9}$ and $G'_0/G'_{0,m} \sim \phi^{2.2}$ for formulations EF and EFD, displayed in Fig. 6b. Scaling laws have been widely studied in literature especially for nanocomposites (Cassagnau 2008). For instance, power law dependences of γ_c, G' and G'' on ϕ coincide with filled-systems such as bohemite alumina particles/aqueous medium (Shih et al. 1990), clay suspended either in PMMA (Vermant et al. 2007) or in PP (Domenech et al. 2014), and also silica/polyol (Saint-Michel et al. 2003) suspensions. The power law exponent depends on the interparticle interactions (Cassagnau 2008). Hence, the higher is the power law coefficient, the stronger are the interparticle interactions. Such coefficient has been also used to discriminate the degree of exfoliation and thus the dispersion in clay/PP nanocomposites (Vermant et al. 2007). They also demonstrated that the sample with the lowest power law

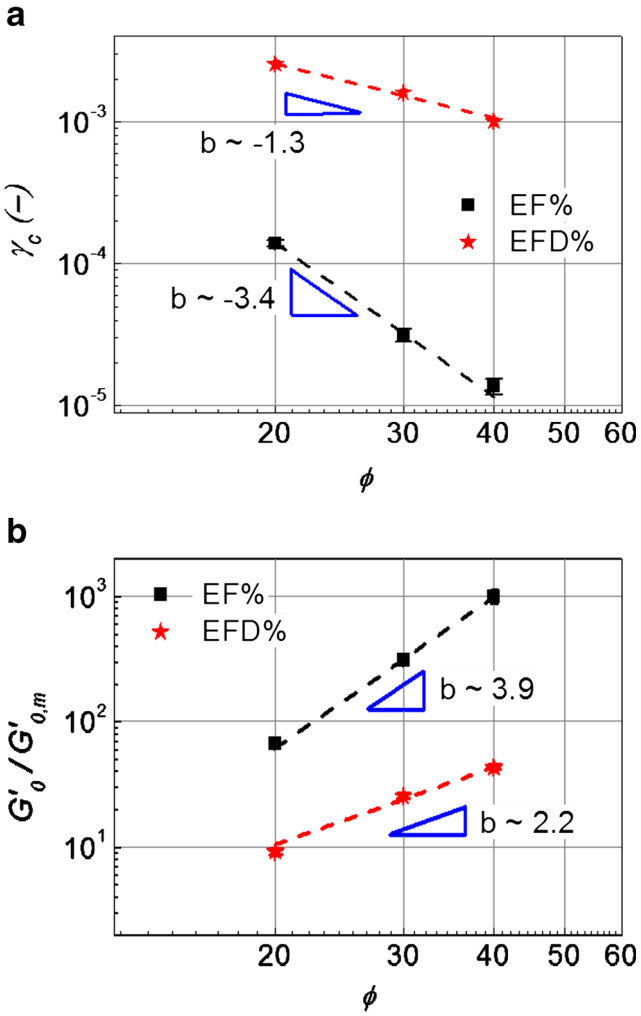

Fig. 6 Power laws relationship for concentrated ferrite suspensions (**a**) critical strain limit (γ_c) and (**b**) storage modulus at the plateau (G'_0) over matrix plateau modulus ($G'_{0,m}$) as a function of filler level (ϕ) for samples with and without the addition of fatty acid

exponent presented a better exfoliation with a more open fractal structure. Here, it is shown again that the fatty acid compound actually reduces interparticle interactions, which may improve the dispersion. However, the latter could not be proven by the tomography analysis which shows very slight differences between the formulations.

Non-linear rheology

Three different capillaries with the same L/D ratio were used to study the slip at the wall. According to the well-known Mooney method (Mooney 1931), wall slip is greater for capillaries with small diameters at same *L*/*D*, because of the larger contribution of the slippage on the total flow.

Figure 7a shows flow curves for the neat matrix, while Fig. 7b displays the results for the sample filled with the highest filler amount (40 vol.%) with and without the addition of the dispersant agent. It is clearly shown that there is no contribution from the surface of the capillary to the flow properties. There is a complete superposition of the three flow curves either for the unfilled polymer or for the concentrated composites. It must be added that EF20 and EFD20 have shown the same trend but these results were omitted in this work for the sake of brevity. Additionally, Fig. 7c–e displays some axial observations from the extrudate. No concentration gradient is observed in these SEM images.

It must be pointed out that the possible flow surface instabilities were not easily observable, especially because our set-up obstructs the direct extrudate observation at the die exit. However, it can be asserted that the extrudates of the filled samples were smooth over all the range of shear rates studied here. This may not be the case for the unfilled matrix, particularly in the moderate and high shear rates range. Smooth surfaces are presented in Fig. 7a–b from the EPPI and EF40 extrudate. From these results, it can be thus concluded that either wall slip or surface wall instabilities do not interfere on the flow behavior of such ferrite composites.

Figure 8 shows steady shear flow properties measured for samples at different solid fractions, as well as, the flow curve of PP matrix (EPPI), depicted by the line. The EPPI flow curve is continuous in all the range of shear rates. The matrix viscosity at low shear rates is purely Newtonian, while by increasing the shear rates, shear thinning behavior appears. Such a behavior is attributed to the exit from the linear to the non-linear domain, in which gradual relaxation of the physical entangled network occurs due to chain stretch and motion (Milner 1996). Figure 8 compiles the filled flow curves for samples (**a**) with and (**b**) without the dispersant agent. First, it is noted that in the non-linear regime, very small differences among the flow curves are evidenced, as it has been observed in rotational flows at high shear rates. Next, it can be clearly seen that for $\dot{\gamma} \to 0$ or $\dot{\gamma} \to \infty, \eta(\dot{\gamma})$ displays higher deviation from the matrix behavior. On the one hand, at high shear rates, the absolute value of the slope decreases and the pseudoplasticity index (n) increases with increasing ϕ. On the other hand, at low shear rate, a deviation from the zero-shear viscosity appears, giving rise to an increase in the slope when increasing ϕ.

Figure 9**a**–**d** displays the shear viscosity at given filler level for samples with and without the dispersant in the formulation. Two process windows can be differentiated in these figures: 10^0 to 10^2 s^{-1} and 10^2 to 10^4 s^{-1}. In the first one, the dispersant agent acts as a lubricant, promoting slip between particles, decreasing particle interactions and thus, decreasing the shear viscosity (Larson 1999). On the second process window, almost no difference between both formulations was observed. Only EF40 and EFD40 showed a significant decrease in viscosity in both process windows, being more significant at low shear rates. Nevertheless, both formulations show similar power law behaviors at high shear rates. This means that the behavior at high shear rates is governed by the same

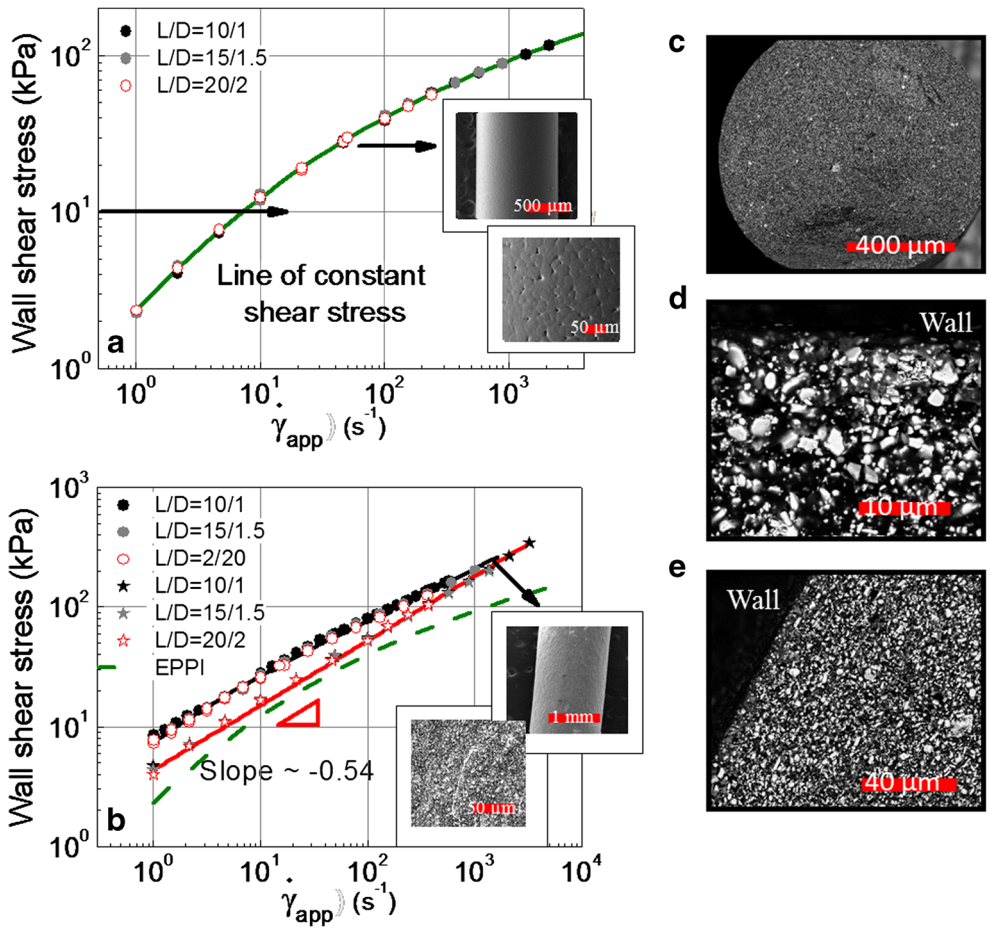

Fig. 7 On the left, wall shear stress versus apparent shear rate for (**a**) unfilled PP (*EPPI*) and (**b**) EF40 without (*circle symbol*) and with (*star symbol*) the addition of the fatty acid at 190 °C, the *dashed line* represents the EPPI matrix behavior, L/D = 10/1, 1.5/15, 2/20, and radial SEM observations of the extrudate EPPI and EF40 at high and small magnification. On the right, axial SEM observations of the (**c**) extrudate (**d**) EF40, and (**e**) EFD40 at 3000 s^{-1}. EFD40 follows a power law model ($\sigma = K\dot{\gamma}^n$) in all the range of shear rates

mechanism. In the same way, lower filled composites show the same slope and thus similar behavior. Special attention should be taken when considering Fig. 9a. Surprisingly, at low shear rates, EFD10 presents a lower viscosity compared to that one of the pure matrix. However, it is important to remember that the reference matrix is only composed of PP + 1 wt.% of irganox. Hence, such decrement may be due to a small excess of dispersant that was not able to be adsorbed onto the particle surface. It may modify the matrix behavior, acting as a plasticizer. Therefore, when $\phi \geq 20\,\% \approx \phi_c$, the interparticle interactions suppress such effect.

To highlight the results, the viscosity of the suspension, $\eta_s(\dot{\gamma})$, has been divided by the viscosity of the melt polymer, $\eta_m(\dot{\gamma})$, at the given shear rate, in order to normalize by the matrix contribution. The results reveal that the dependency of $\eta_r(\dot{\gamma}) = \eta_s(\dot{\gamma})/\eta_m(\dot{\gamma})$ on $\dot{\gamma}$, exhibits three distinct regimes as Fig. 10 shown. Each of these regimes are associated to low, moderate, and high shear rates. At low shear rates, the macrostructure is dominated by the particle interactions. The more is the filler amount, the higher is the deviation of the viscosity from the zero-shear viscosity. Such microstructure is attributed to a particle network. Next, $\eta_r(\dot{\gamma})$ decreases to attain a minimum, revealing a shear thinning behavior which comes strictly from the ferrite phase. In fact, flow lines start to disturb ferrite particles orientation, which provokes an alignment and thus rupture of the network. In this zone, the filled composites present the closest behavior to that of the matrix. This evidences a completely destroyed structure, in which the viscosity contribution from the particles is the lowest. Finally, at high shear rates, $\eta_r(\dot{\gamma})$ starts to rise again. The higher is the filler level, the lower is the onset of non-linearity. Such a dramatic increase may be attributed to a new microstructure imposed by the high flow rate, thus an attenuation on the shear thinning behavior is clearly observed, which could indicate to the possible onset on shear thickening behavior. The latter can be also observed by illustrating the normalized shear viscosity as a function of the wall shear stress (Fig. 11). In contrast to Fig. 10, this representation of the data presents a very slight deviation of the filled composites from the pure matrix at low shear rates.

It has been evidenced that some concentrated colloidal suspensions and non-Brownian suspensions (suspended in a low molar mass liquid) shown an abrupt increase in the viscosity above a critical shear rate or wall shear stress (Fall et al. 2012). However, analogous works on highly filled molten polymers reported that, at high shear rates, highly filled samples either

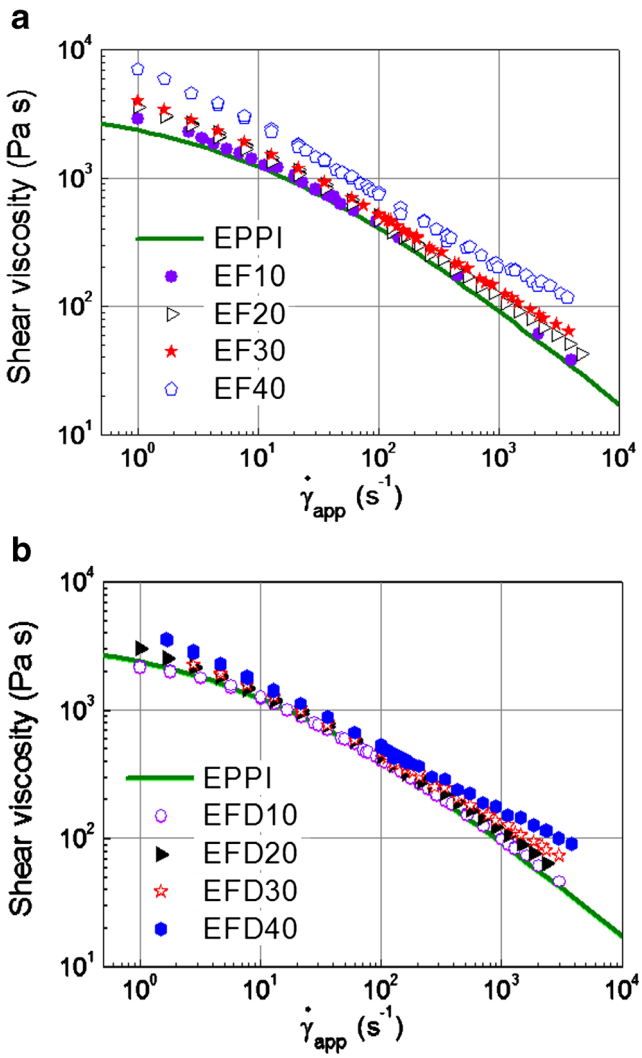

Fig. 8 Relationship between the shear viscosity and shear rate, $\dot{\gamma}$, of filled composites (**a**) without and (**b**) with the addition of the fatty acid. The *line* represents the unfilled matrix (EPPI). Steady state test performed at 190 °C, L/D = 20/1

converge to the matrix flow curve (Chan et al. 1978; Hornsby and Mthupha 1994; A. Ramazani et al. 2001; Kim et al. 2004) or present the same power law behavior to that of the matrix (Minagawa and White 1976; Czarnecki and White 1980; Saini et al. 1985; Poslinski et al. 1988a; Osman et al. 2004) (same slope). It is generally believe that at very high shear rates (or shear stresses) the effect of the polymer matrix is much larger, totally suppressing the interparticle interactions. Here, we showed that, at high shear rates, the particle configuration change, leading to a new created micro-structure which opposes a certain restriction to flow. The same behavior was observed for particles covered by the fatty acid.

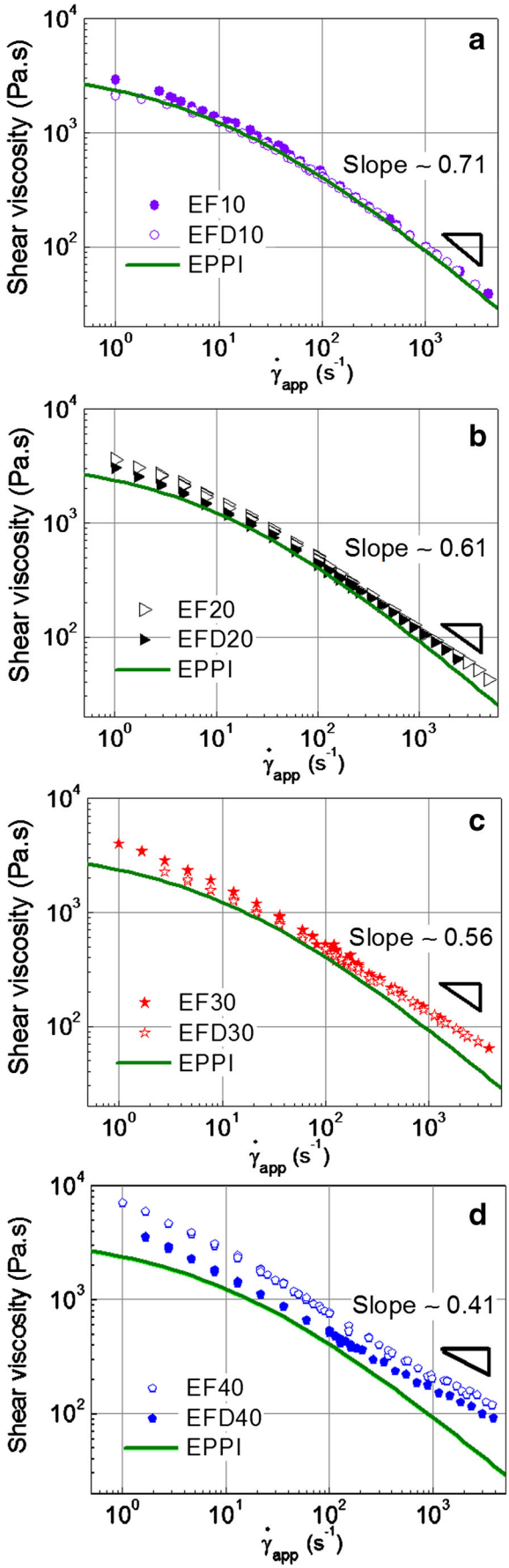

Fig. 9 Comparison between samples with and without the addition of dispersant filled with (**a**) 10 vol.% (**b**) 20 vol.% (**c**) 30 vol.%, and (**d**) 40 vol.%. Steady state test performed at 190 °C, L/D = 20/1

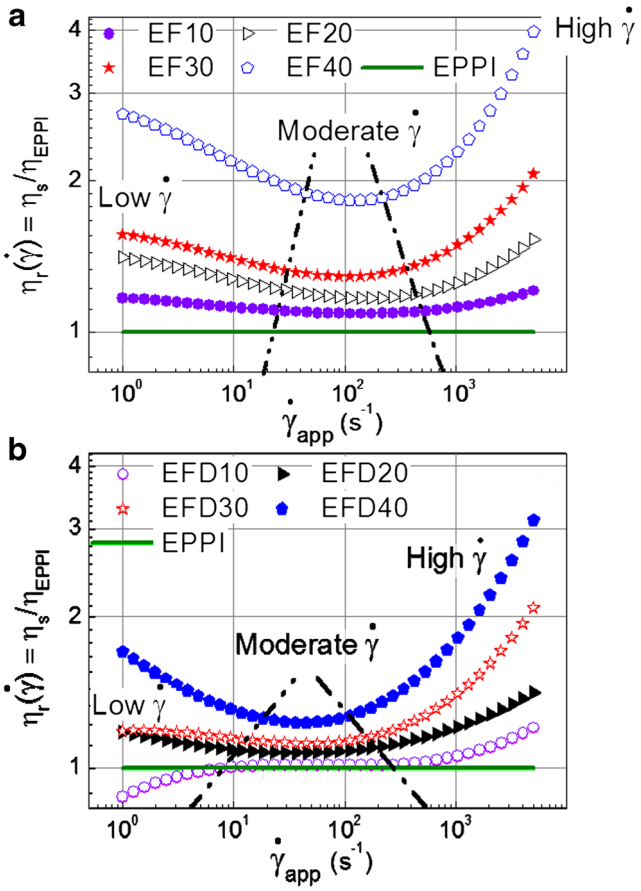

Fig. 10 Dimensionless shear viscosity as a function of the shear rate, normalized by the shear viscosity of the pure matrix at given shear rate. Formulations (**a**) without and (**b**) with the dispersant agent

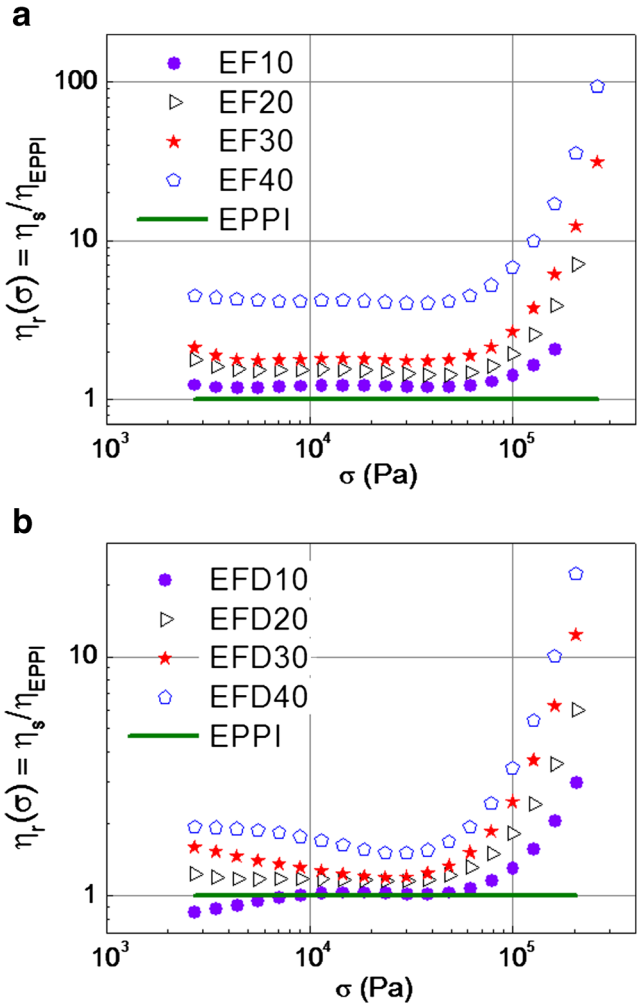

Fig. 11 Dimensionless shear viscosity as a function of the shear stress, normalized by the shear viscosity of the pure matrix at given wall shear stress. Formulations (**a**) without and (**b**) with the dispersant agent

Based on these results, it can be concluded that the addition of the dispersant agent modifies the flow behavior (Fig. 7b), decreases particles interactions and thus decreases the viscosity of the mixture (Fig. 9d). Such decrement is most important in the low shear rate process window. It can be expected that high shear rates induce fatty acid migration from the ferrite surface to the bulk, rather than to the die wall. The diffusion of the fatty acid to the wall might be restricted by the presence of the particles.

Conclusions

In this work, we have studied the flow nature of ferrite suspensions in the linear and the non-linear regime for samples filled with 10, 20, 30, and 40 vol.%, with and without the addition of a commercial dispersant SDP310. Under dynamic flows, it was observed that γ_c and $G'_0/G'_{0,m}$ follow power law dependencies with ϕ. Such dependency is most pronounced for samples without the fatty acid compound. The dispersant agent actually reduces the moduli values and increases the linear domain. Under non-linear shear in capillary rheometer, the flow properties were found to do not depend on the diameter of the die. Wall slip contribution is negligible at the shear rates studied here. The nature of the flow was divided into three distinct sections: low, moderate, and high shear rates. Such region presents very distinctive characteristics and has been attributed to distinct micro-structures formed due to flow. At low shear rates, a deviation from the zero-shear viscosity is observed which might correspond to a network structure. Moderate shear rates destroy particle network and thus particles are oriented in the flow direction, by increasing interparticle distances. In such region, the behavior is the closest to the unfilled polymer. Finally, high shear rates create a new microstructure which attenuates the shear thinning behavior. Particles orient in the flow direction and may form local clusters which restrict the flow. A possible onset on shear thickening is put in evidence. When adding a dispersant agent, shear viscosity presented lower values at fixed ϕ, at low shear rates. At high shear rates, only the EF40% and EFD40% showed a remarkable decrease on viscosity. From this, it can

be also concluded that by adding a fatty acid, particle interactions are decreased and thus the shear viscosity, which will improve the extrudability and the injection moldability of these materials.

Acknowledgments The authors thank Mr. Dubois who performed the tomography analysis. The scanning electron microscopy observations were carried out at the Technological Centre of Microstructures, Claude Bernard University of Lyon 1. The authors thank them for their technical support and help. This work was funded by Hutchinson Research Center thanks to the Laboratory of Polymer Materials Engineering (IMP)-Hutchinson joint laboratory.

References

A. Ramazani S, Ait-Kadi A, Grmela M (2001) Rheology of fiber suspensions in viscoelastic media: experiments and model predictions. J Rheol 45:945–962. doi:10.1122/1.1378026

Ahn S, White JL (2004) Wall effects on flow of polymer/particulate/(carboxylic acid) in dies and rheometers. J Appl Polym Sci 91: 651–658. doi:10.1002/app.13109

Aral BK, Kalyon DM (1995) Rheology and extrudability of very concentrated suspensions: effects of vacuum imposition. Plast Rubber Compos Process Appl 4:201–210

Ariffin A, Jikan SS, Samsudin MSF et al (2006) Melt elasticity phenomenon of multicomponent (talc and calcium carbonate) filled polypropylene. J Reinf Plast Compos 25:913–923. doi:10.1177/0731684406063550

Armistead CG, Tyler AJ, Hambleton FH et al (1969) Surface hydroxylation of silica. J Phys Chem 73:3947–3953. doi:10.1021/j100845a065

Azoug A, Nevière R, Pradeilles-Duval R-M, Constantinescu A (2014) Influence of crosslinking and plasticizing on the viscoelasticity of highly filled elastomers. J Appl Polym Sci 131:40392(1-9). doi:10.1002/app.40392

Barnes HA (2003) Review of the rheology of filled viscoelastic systems, rheology reviews, the British Society of Rheology. Br Soc Rheol 49

Boudenne A, Ibos L, Fois M et al (2005) Electrical and thermal behavior of polypropylene filled with copper particles. Compos Part Appl Sci Manuf 36:1545–1554. doi:10.1016/j.compositesa.2005.02.005

Bravo VL, Hrymak AN, Wright JD (2004) Study of particle trajectories, residence times and flow behavior in kneading discs of intermeshing co-rotating twin-screw extruders. Polym Eng Sci 44:779–793. doi:10.1002/pen.20070

Burnat D, Ried P, Holtappels P et al (2010) The rheology of stabilised lanthanum strontium cobaltite ferrite Nanopowders in organic medium applicable as screen printed SOFC cathode layers. Fuel Cells 10:156–165. doi:10.1002/fuce.200900014

Cassagnau P (2003) Payne effect and shear elasticity of silica-filled polymers in concentrated solutions and in molten state. Polymer 44: 2455–2462. doi:10.1016/S0032-3861(03)00094-6

Cassagnau P (2008) Melt rheology of organoclay and fumed silica nanocomposites. Polymer 49:2183–2196. doi:10.1016/j.polymer.2007.12.035

Cassagnau P (2013) Linear viscoelasticity and dynamics of suspensions and molten polymers filled with nanoparticles of different aspect ratios. Polymer 54:4762–4775. doi:10.1016/j.polymer.2013.06.012

Chan Y, White JL, Oyanagi Y (1978) A fundamental study of the rheological properties of glass-fiber-reinforced polyethylene and polystyrene melts. J Rheol 22:507–524. doi:10.1122/1.549486

Czarnecki L, White JL (1980) Shear flow rheological properties, fiber damage, and mastication characteristics of aramid-, glass-, and cellulose-fiber-reinforced polystyrene melts. J Appl Polym Sci 25: 1217–1244. doi:10.1002/app.1980.070250623

Dasgupta S (1988a) Degree and stability of magnetic dispersions: sedimentation, rheological, and magnetic properties. J Colloid Interface Sci 121:208–213. doi:10.1016/0021-9797(88)90424-9

Dasgupta S (1988b) Interaction characteristics of magnetic particles with surfactants, solvents, and binder resins. J Colloid Interface Sci 124: 22–27. doi:10.1016/0021-9797(88)90320-7

Denn MM (2001) Extrusion instabilities and wall slip. Annu Rev Fluid Mech 33:265–287. doi:10.1146/annurev.fluid.33.1.265

Domenech T, Zouari R, Vergnes B, Peuvrel-Disdier E (2014) Formation of fractal-like structure in organoclay-based polypropylene nanocomposites. Macromolecules 47:3417–3427. doi:10.1021/ma5001354

Fall A, Bertrand F, Ovarlez G, Bonn D (2012) Shear thickening of cornstarch suspensions. J Rheol 56:575–591. doi:10.1122/1.3696875

Fall A, de Cagny H, Bonn D et al (2013) Rheology of sedimenting particle pastes. J Rheol 57:1237–1246. doi:10.1122/1.4809732

Feger C, Gelorme JD, McGlashan-Powell M, Kalyon DM (2005) Mixing, rheology, and stability of highly filled thermal pastes. IBM J Res Dev 49:699–707. doi:10.1147/rd.494.0699

Fiske T, Gokturk HS, Yazici R, Kalyon DM (1997) Effects of flow induced orientation of ferromagnetic particles on relative magnetic permeability of injection molded composites. Polym Eng Sci 37: 826–837. doi:10.1002/pen.11725

Franceschini A, Filippidi E, Guazzelli E, Pine DJ (2014) Dynamics of non-Brownian fiber suspensions under periodic shear. Soft Matter 10:6722–6731. doi:10.1039/c4sm00555d

Gao F, Yang S, Hao P, Evans JRG (2011) Suspension stability and fractal patterns: a comparison using hydroxyapatite. J Am Ceram Soc 94: 704–712. doi:10.1111/j.1551-2916.2010.04149.x

Gassiot-Talabot A (2015) Renforcement d'un poly(oxyéthylène) par dispersion de whiskers de cellulose en voie fondue : contraintes et alternatives. Dissertation, Jean Monnet University

Gulmus SA, Yilmazer U (2005) Effect of volume fraction and particle size on wall slip in flow of polymeric suspensions. J Appl Polym Sci 98:439–448. doi:10.1002/app.21928

Haworth B, Khan SW (2005) Wall slip phenomena in talc-filled polypropylene compounds. J Mater Sci 40:3325–3337. doi:10.1007/s10853-005-0424-2

Hidber PC, Graule TJ, Gauckler LJ (1997) Influence of the dispersant structure on properties of electrostatically stabilized aqueous alumina suspensions. J Eur Ceram Soc 17:239–249. doi:10.1016/S0955-2219(96)00151-3

Hornsby PR, Mthupha A (1994) Rheological characterization of polypropylene filled with magnesium hydroxide. J Mater Sci 29:5293–5301. doi:10.1007/BF01171538

Hristov V, Takács E, Vlachopoulos J (2006) Surface tearing and wall slip phenomena in extrusion of highly filled HDPE/wood flour composites. Polym Eng Sci 46:1204–1214. doi:10.1002/pen.20592

Kalyon DM (2005) Apparent slip and viscoplasticity of concentrated suspensions. J Rheol 49:621–640. doi:10.1122/1.1879043

Kalyon DM, Aktaş S (2014) Factors affecting the rheology and processability of highly filled suspensions. Annu Rev Chem Biomol Eng 5: 229–254. doi:10.1146/annurev-chembioeng-060713-040211

Kaully T, Siegmann A, Shacham D (2007) Rheology of highly filled natural CaCO3 composites. I. Effects of solid loading and particle size distribution on capillary rheometry. Polym Compos 28:512–523. doi:10.1002/pc.20308

Kim K-J, White JL, Eun Shim S, Choe S (2004) Effects of stearic acid coated talc, CaCO3, and mixed talc/CaCO3 particles on the rheological properties of polypropylene compounds. J Appl Polym Sci 93:2105–2113. doi:10.1002/app.20686

Kim H, Abdala AA, Macosko CW (2010) Graphene/polymer nanocomposites. Macromolecules 43:6515–6530. doi:10.1021/ma100572e

Larson RG (1999) The structure and rheology of complex fluids. OUP USA, New York

Li TQ, Wolcott MP (2005) Rheology of wood plastics melt. Part 1. Capillary rheometry of HDPE filled with maple. Polym Eng Sci 45:549–559. doi:10.1002/pen.20308

Lusiola T, Scharf D, Graule T, Clemens F (2014) Low shear compounding process for thermoplastic fabrication of ferroelectric lead-free fibres. J Eur Ceram Soc 34:2265–2274. doi:10.1016/j.jeurceramsoc.2014.02.036

Merabia S, Sotta P, Long DR (2008) A microscopic model for the reinforcement and the nonlinear behavior of filled elastomers and thermoplastic elastomers (Payne and Mullins effects). Macromolecules 41:8252–8266. doi:10.1021/ma8014728

Milner ST (1996) Relating the shear-thinning curve to the molecular weight distribution in linear polymer melts. J Rheol 40:303–315. doi:10.1122/1.550742

Minagawa N, White JL (1976) The influence of titanium dioxide on the rheological and extrusion properties of polymer melts. J Appl Polym Sci 20:501–523. doi:10.1002/app.1976.070200222

Moloney VMB, Parris D, Edirisinghe MJ (1995) Rheology of zirconia suspensions in a nonpolar organic medium. J Am Ceram Soc 78:3225–3232. doi:10.1111/j.1151-2916.1995.tb07958.x

Mooney M (1931) Explicit formulas for slip and fluidity. J Rheol 2:210–222. doi:10.1122/1.2116364

Navarrete RC, Scriven LE, Macosko CW (1996) Rheology and structure of flocculated iron oxide suspensions. J Colloid Interface Sci 180:200–211. doi:10.1006/jcis.1996.0290

Osman MA, Atallah A, Schweizer T, Öttinger HC (2004) Particle–particle and particle-matrix interactions in calcite filled high-density polyethylene—steady shear. J Rheol 48:1167–1184. doi:10.1122/1.1784782

Poslinski AJ, Ryan ME, Gupta RK et al (1988a) Rheological Behavior of filled polymeric systems I. Yield stress and shear-thinning effects. J Rheol 32:703–735. doi:10.1122/1.549987

Poslinski AJ, Ryan ME, Gupta RK et al (1988b) Rheological Behavior of filled polymeric systems II. The effect of a bimodal size distribution of particulates. J Rheol 32:751–771. doi:10.1122/1.549991

Potanin A, N. K. Nelson, Jr. (2003) Formulation effects on magnetic mix microstructure based on rheological, magnetic susceptability, and particle size measurements. J Rheol 47:389–412. doi:10.1122/1.1538607

Ried P, Lorenz C, Brönstrup A et al (2008) Processing of YSZ screen printing pastes and the characterization of the electrolyte layers for anode supported SOFC. J Eur Ceram Soc 28:1801–1808. doi:10.1016/j.jeurceramsoc.2007.11.018

Rueda MM, Fulchiron R, Cassagnau P et al (2016) Structuring of non-Brownian ferrite particles in molten polypropylene: viscoelastic analysis. J Rheol 60:1245–1255. doi:10.1122/1.4963801

Rueda MM, Auscher M-C, Fulchiron R et al (2017) Rheology and applications of highly filled polymers: a review of current understanding. Prog Polym Sci 66:22–53. doi:10.1016/j.progpolymsci.2016.12.007

Saini DR, Shenoy AV, Nadkarni VM (1985) Effect of surface treatments on rheological, mechanical and magnetic properties of ferrite-filled polymeric systems. Polym Eng Sci 25:807–811. doi:10.1002/pen.760251304

Saini DR, Shenoy AV, Nadkarni VM (1986) Melt rheology of highly loaded ferrite-filled polymer composites. Polym Compos 7:193–200. doi:10.1002/pc.750070402

Saint-Michel F, Pignon F, Magnin A (2003) Fractal behavior and scaling law of hydrophobic silica in polyol. J Colloid Interface Sci 267:314–319. doi:10.1016/j.jcis.2003.07.018

Shih W-H, Shih WY, Kim S-I et al (1990) Scaling behavior of the elastic properties of colloidal gels. Phys Rev A 42:4772

Soltani F, Yilmazer Ü (1998) Slip velocity and slip layer thickness in flow of concentrated suspensions. J Appl Polym Sci 70:515–522. doi:10.1002/(SICI)1097-4628(19981017)70:3<515::AID-APP13>3.0.CO;2-#

Suwardie H, Yazici R, Kalyon DM, Kovenklioglu S (1998) Capillary flow behaviour of microcrystalline wax and silicon carbide suspension. J Mater Sci 33:5059–5067. doi:10.1023/A:1004423411227

Vermant J, Ceccia S, Dolgovskij MK et al (2007) Quantifying dispersion of layered nanocomposites via melt rheology. J Rheol 51:429–450. doi:10.1122/1.2516399

Voillequin B, Ayme-Perrot D, Dufour B, Sonntag P (2013) Cathode for a cell of a lithium-ion battery, its manufacturing process and the battery incorporating it. Patent US20130183577 A1

Walberer JA, McHugh AJ (2001) The linear viscoelastic behavior of highly filled polydimethylsiloxane measured in shear and compression. J Rheol 45:187–201. doi:10.1122/1.1332386

Yang M-C, Scriven LE, Macosko CW (1986) Some rheological measurements on magnetic iron oxide suspensions in silicone oil. J Rheol 30:1015–1029. doi:10.1122/1.549892

Yilmazer U, Kalyon DM (1989) Slip effects in capillary and parallel disk torsional flows of highly filled suspensions. J Rheol 33:1197. doi:10.1122/1.550049

Zürcher S, Graule T (2005) Influence of dispersant structure on the rheological properties of highly-concentrated zirconia dispersions. J Eur Ceram Soc 25:863–873. doi:10.1016/j.jeurceramsoc.2004.05.002